Proceedings of the Combustion Institute 42 (2026) 106158

Contents lists available at ScienceDirect

Proceedings of the Combustion Institute

journal homepage: www.elsevier.com/locate/proci

Iron as a recyclable energy carrier: Redox cycling of iron oxide pellets for hydrogen storage

Anna Knapp, Robin Flügel, Felix Straub, Olaf Deutschmann *

Institute for Chemical Technology and Polymer Chemistry, Karlsruhe Institute of Technology, 76131 Karlsruhe, Germany

ARTICLE INFO

Keywords:
Metal fuels
Iron redox cycling
Hydrogen storage
Steam-iron process

ABSTRACT

The reversible storage of hydrogen in metal oxides via the steam-iron process offers a promising pathway for large-scale, carbon-free energy storage. In this study, the redox performance and mechanical stability of iron oxide-based pellets were investigated over ten redox cycles. Pelletization produced mechanically robust pellets (1–2 mm) suitable for fixed-bed operation. Trends previously observed for iron oxide powders (100-200 µm), such as sintering-induced deactivation and stabilization by dopants, were confirmed in pellet form. Remarkably, iron oxide of lower purity containing trace amounts of Al and Cr exhibited nearly constant H_2 production over ten cycles, which can be attributed to the combined stabilizing effects of minor impurities, a primary particle morphology less prone to sintering, and crack formation during redox cycling that enhances gas transport within the pellets. Increasing the induration temperature of Al-modified iron oxide to 1300 °C significantly improved the mechanical integrity of the pellets and both H_2 production and porosity increased with cycle number. These findings demonstrate the potential of additive-stabilized iron oxide pellets as durable and recyclable hydrogen storage material.

Novelty and significance statement: This study bridges the gap between powder-scale research and practical fixed-bed operation by systematically evaluating pelletized iron oxides in the steam-iron process. It demonstrates how pellet microstructure, induration temperature, and presence of stabilizing additives govern long-term redox stability under cyclic conditions. Trace-level impurities can provide stabilization comparable to deliberate modification, highlighting the potential of low-cost, naturally occurring iron oxides. The findings support the development of stable, cost-effective iron-based materials for cyclic energy storage.

1. Introduction

Metal fuels, especially iron, have gained attention for large-scale temporal and seasonal energy storage due to their high volumetric energy density and recyclability [1–4]. Energy storage in iron occurs via thermochemical reduction of iron oxides using preferentially green hydrogen [5,6]. Energy release can proceed through direct combustion in air to produce heat [7,8], or via steam oxidation to generate hydrogen for direct use or power production fuel cell [9]. The resulting iron oxides remain solid under ambient conditions, enabling easy collection and recyclability, supporting a closed-loop, carbon-free energy storage cycle [10,11].

The concept of using iron for hydrogen generation dates back to the 19th century, when the steam-iron process was first employed commercially [12,13]. For hydrogen storage application, thermodynamic studies suggest optimal temperature windows of > 420 °C for reduction and 100 °C to 500 °C for oxidation [14]. The redox cycle proceeds between Fe and Fe_3O_4 and therefore exhibits a theoretical maximum hydrogen storage of 4.8 wt.—% in iron [15].

According to Brinkman et al. [14], the energy demand for hydrogen storage via the steam-iron process is approximately 27 % of the lower heating value (LHV) of hydrogen, depending on the exact process conditions. This places it within the same range as most chemical hydrogen storage methods, including ammonia (22 %) and liquid organic hydrogen carriers (25 % to 27 %), while metal hydrides such as MgH_2 require around 33 % relative to the LHV. In comparison, liquid hydrogen storage requires approximately 18 % of the LHV, whereas the energy demand for compressed hydrogen storage at 700 bar is significantly lower at about 6 % to 8 %. [14] However, physical hydrogen storage approaches are associated with drawbacks such as limited volumetric energy density in compressed systems and boil-off losses in cryogenic storage [16].

* Corresponding author.
E-mail address: deutschmann@kit.edu (O. Deutschmann).

https://doi.org/10.1016/j.proci.2026.106158
Received 13 March 2026; Accepted 7 June 2026
Available online 3 July 2026

Beyond energetic considerations, the practical viability of hydrogen storage systems is strongly determined by their long-term cycling stability. It is critical to maintain performance over multiple cycles, as repeated reduction and oxidation lead to structural degradation through sintering and phase transformations [17,18]. Previous studies [15,19–21] have shown that material stabilization can be achieved through modification with stabilizing additives. The addition of small amounts of dopants, such as aluminium, chromium, calcium and molybdenum, can mitigate sintering and improve redox stability by forming mixed oxides or secondary phases.

While prior studies largely employed powders in thermogravimetric setups [15,19–21], pellets were used in this work for practical reasons. Nevertheless, the long-term stability and mechanical integrity of pelletized forms for fixed-bed operation remain insufficiently explored. This study investigates the cyclic redox behavior of iron oxide pellets in the steam-iron process using a fixed-bed reactor. Alongside previously studied Mo- and Al-modified oxides [21], an impure iron oxide containing trace Al and Cr is examined to assess the potential of naturally occurring materials with inherent stabilizers, reducing the need for synthetic modification and advancing iron's use as a recyclable hydrogen storage medium.

2. Experimental setup and methods

2.1. Pellet preparation

A series of iron oxide and modified iron oxide pellets were prepared. Modified iron oxides with 5 mol% Al or Mo were synthesized by incipient-wetness impregnation of Fe_2O_3 powder (99.9 %, ThermoFisher) using aqueous solutions of $Al(NO_3)_3 \cdot 9\,H_2O$ (min. 98.5 %, Merck) or $(NH_4)_6Mo_7O_{24}$ (min. 99.0 %, Merck). After impregnation, samples were dried for 24 h at 60 °C and calcined in air for 5 h at 700 °C. An additive concentration of 5 mol% was chosen, as studies showed that it provides a balance between stability and H_2 storage density [20].

Pellets were prepared from high-purity Fe_2O_3 powder (99.9 %, ThermoFisher), Mo-, Al-modified Fe_2O_3 and lower-purity Fe_2O_3 (98 %, ThermoFisher). The samples are denoted as FeOx, FeOx-Mo, FeOx-Al and FeOx-98, respectively. According to the supplier, FeOx-98 contains 585 ppm Al, 453 ppm Cr, and 151 ppm Na as main impurities.

The iron oxide powders were pelletized using a laboratory pelletizing disk with a diameter of 0.4 m (inclination 52°, 40 min^{-1}) and deionized water, as these parameters were identified as optimal by Huber et al. [22]. 1 wt.—% lactose was used as binder. The green pellets were dried for 20 h at 75 °C. As the dried pellets are too fragile for handling, they require hardening through thermal treatment, commonly referred to as induration in the context of pelletization [23,24]. The pellets were indurated in air for 5 h at 700 °C. Al-modified iron oxide pellets were also indurated to 1300 °C for 1 h, hereafter abbreviated as FeOx-Al(HT).

The pellets were sieved to a 1 mm to 2 mm fraction for fixed-bed experiments.

2.2. Evaluation of the hydrogen storage performance

The cyclic reduction and oxidation of the iron oxide pellets were performed in a fixed-bed reactor. The experimental setup is illustrated in Fig. 1. The quartz reactor (8 mm i.d.) was filled with 500 ± 3 mg of iron oxide pellets secured with quartz wool, which formed a bed of approximately 10 mm length. The reactor was placed in a uniformly heated furnace (HTM Reetz), and temperature was monitored by two N-type thermocouples positioned 1 mm upstream and downstream of the bed. Gas flows of H_2 and N_2 were controlled by mass flow controllers (MFC, Bronkhorst), and water was supplied and vaporized using a Liquiflow (LFC, Bronkhorst) and Controlled Evaporation Mixer (CEM, Bronkhorst). The exhaust gas is analyzed by a Fourier-transformation infrared spectrometer (FTIR, MKS Instruments) and by a H_2 mass spectrometer (H_2-MS, V&F). Research data management was conducted using the Adacta software [25].

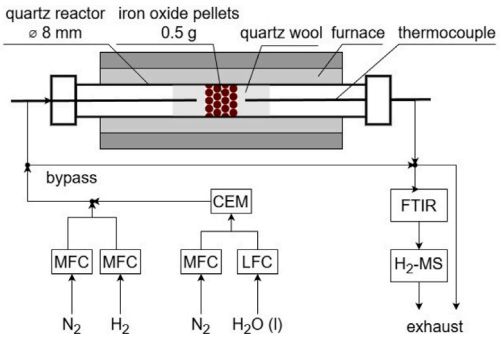

Fig. 1. Schematic representation of the experimental setup for the evaluation of the hydrogen storage performance.

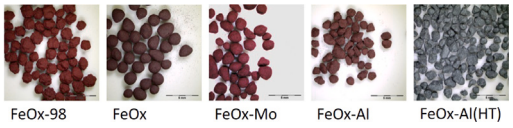

Fig. 2. FeOx Pellets under light microscope.

Experiments were conducted with a total gas flow of 500 mL min^{-1} under standard conditions. Each cycle consisted of reduction with 5 vol.—% H_2 for 90 min and oxidation with 20 vol.—% H_2O for 20 min, balanced with N_2. The reactor was purged with N_2 for 10 min before and between cycles. Each sample was tested over ten consecutive cycles.

All steam-iron process experiments were conducted at 600 °C, which represents a balanced compromise between sufficiently high reaction rates and material stability. This operating temperature was also chosen to enable direct comparison with a previous studies [21]. The present study concentrates on the oxidation step, whereas the reduction behavior of iron oxides has already been comprehensively addressed in literature [26–29]. Hydrogen release during oxidation provides a direct measure of redox performance and material degradation, making the oxidation step a reliable indicator of overall stability.

2.3. Characterization

Light microscopy images of the pellets after induration were recorded with an Olympus SC30 with a 0.67-times magnification.

Compressive strength test were carried out with a Universal Testing Machine 10kN, Hegewald &Peschke. For each sample ten pellets were tested and a mean compressive strength was determined in order to account for the varying pellet size between 1 mm to 2 mm.

Scanning electron microscopy images of the pellet surface were taken using a Zeiss LEO 1530 Gemini with an acceleration voltage of 10 kV. Cross-sectional SEM images of resin-embedded pellets were taken with FEI Quanta 650 with an acceleration voltage of 15 kV.

The specific surface area was measured using a Belsorp Mini II device from Bel Japan Inc. The analysis was performed using 500 mg of each sample. Pretreatment of the samples was performed at 300 °C in vacuum for three hours to remove adsorbed substances.

3. Results

3.1. Pelletization

All powders were successfully pelletized into mechanically robust particles, as shown in Fig. 2.

The resulting pellets withstood a fall onto a steel plate from a height of 0.5 m without visible fragmentation. All pellets indurated at

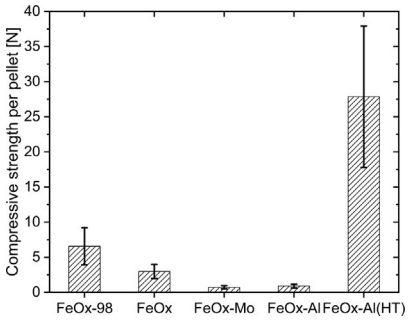

Fig. 3. Mean compressive strength per pellet and their standard deviation of the pellets prepared in this work.

700 °C, but most pronounced in FeOx-Al, exhibited powder abrasion during handling, indicating limited mechanical stability. The mean compressive strength per pellet is shown in Fig. 3. Regarding the pellets indurated at 700 °C, FeOx-98 pellets show the highest compressive strength with 7 N per pellet. In contrast, FeOx-Mo and FeOx-Al pellets exhibited compressive strengths three to four times lower than FeOx pellets, despite being based on the same high-purity iron oxide powder.

Halt et al. [30] reported that additives, which destabilize the particle-water system during pelletization, reflected by a lower zeta potential, lead to weaker, dustier pellets. Aluminum was found to have such a destabilizing effect.

To improve mechanical stability, the induration temperature of the Al-modified pellets was increased to 1300 °C. This temperature was selected because compressive strength typically reaches a maximum in the range of 1250 °C to 1300 °C [24]. Although Mo-modified iron oxide pellets also showed inferior mechanical stability, the induration temperature could not be increased as MoO_3 volatilization occurs above 700 °C [31].

Increasing the induration temperature of Al-modified iron oxide pellets resulted in a distinct color change from red to gray (Fig. 2). This transformation can be associated with the thermally induced color change of hematite, attributed to increased crystallinity and particle size, accompanied by modifications in the electronic structure [32]. In addition, FeOx-Al(HT) pellets showed no abrasion during handling and achieved a mean compressive strength of 28 N per pellet. Thus, induration at 1300 °C increased the compressive strength of Al-modified pellets by a factor of 31 compared to their equivalents indurated at 700 °C.

3.2. Cycling experiments

In order to evaluate the hydrogen storage and release performance of the prepared iron oxide pellets, cyclic redox experiments were subsequently conducted. This study focuses on the oxidation process. The H_2 concentration over time during the oxidation of the iron oxide pellets in the first and tenth cycle is shown in Fig. 4.

All iron oxide pellets exhibit a rapid initial hydrogen production followed by a gradual decline. However, the maximum hydrogen concentration and oxidation duration vary among the different oxides.

In the initial cycle, pure FeOx shows the slowest oxidation, reaching a maximum H_2 concentration of 7 vol.—%. After the initial decrease a plateau is reached with a local peak in H_2 concentration around 10 min. H_2 production ceased after 16 min. In the tenth cycle, the peak H_2 concentration decreased by 77 %. 20 min were insufficient for complete oxidation, as H_2 evolution stabilized at a low level.

Qualitatively, very similar concentration profiles were obtained in a previous study [21] investigating the redox behavior of iron oxide powders (particle size = 100 µm to 200 µm) in the fixed-bed reactor shown in Fig. 1. These concentration profiles indicate that the oxidation

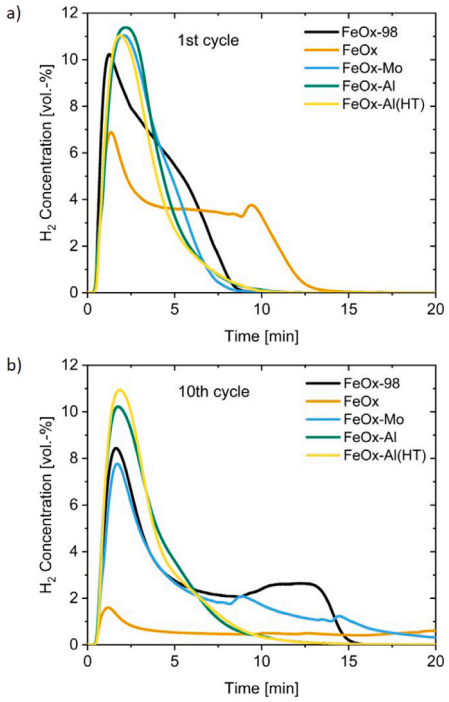

Fig. 4. H_2 concentration over time during oxidation with different additives during the first (a) and tenth (b) redox cycle.

may transition from an initially rapid, kinetically controlled regime at the pellet surface and within open pores to a diffusion-limited regime [33]. During the first cycle, the surface area accessible to the reacting gas remains significantly larger than in the tenth cycle (Table 1). Since sintering is the primary cause of deactivation during redox cycling of iron oxides [18], the accessible surface area decreases with increasing cycle number. Consequently, the contribution of fast surface oxidation diminishes with increasing cycle number. The secondary peaks observed in the H_2 concentration profiles may be attributed to crack formation during the later stages of oxidation. In magnetite, such cracking is frequently reported and arises from mechanical stresses induced by volumetric expansion during oxidation in the brittle material [34]. The formation of these cracks exposes previously unreacted iron surfaces to the gas phase, leading to a temporary increase in the oxidation rate.

In contrast, the modified samples displayed faster initial oxidation. In the first cycle, all modified iron oxides exhibit very similar concentration profiles, reaching peak concentrations of 11 vol.—% and completing oxidation after about 11 min. After ten cycles, the concentration profiles of the modified iron oxides become clearly distinguishable. The peak concentration decreased by 30 % for FeOx-Mo and 10 % for FeOx-Al, while FeOx-Al(HT) maintained a stable initial oxidation rate. For both Al-modified samples, the duration of H_2 evolution increased by about 6 min, showing a similar, but slightly widened concentration profile compared to the first cycle. In contrast, FeOx-Mo exhibited incomplete oxidation within 20 min, and showed two local maxima at approximately 8 and 15 min, indicating that crack formation occurred during oxidation and that diffusion limitations become increasingly significant with increasing cycle number.

In previous work [21] using powders, faster oxidation and more stable concentration profile with respect to the cycle number of Al- than Mo-modified oxides was also observed. One possible explanation is that Al-doping may enhance O^{2-}-ion diffusion and promote H_2O dissociation [19], thereby accelerating oxidation, as the chemisorption of water is considered the rate-limiting step in the initial stage of the process [35]. The stabilizing mechanisms of Al and Mo reported in

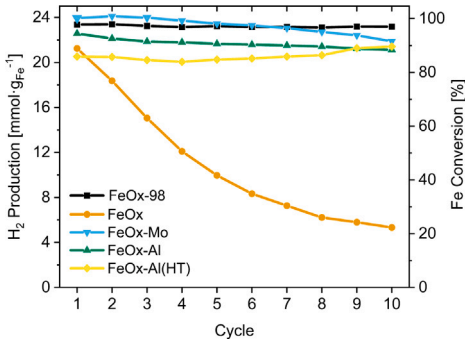

Fig. 5. Accumulative H_2 production during oxidation with different additives over ten redox cycles.

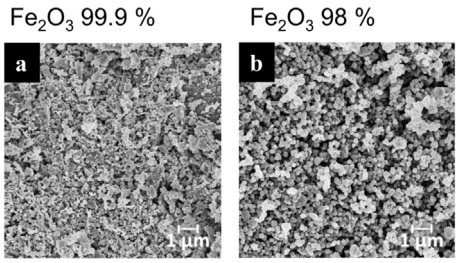

Fig. 6. Surface SEM images of the pelletized (a) Fe_2O_3 (99.9 % purity) and (b) Fe_2O_3 (98 % purity).

the literature involve the formation of mixed ferrites, $FeAl_2O_4$ and $Mo_xFe_{3-x}O_4$ [36,37], which mitigate neck growth between adjacent particles [18]. The formation of $FeAl_2O_4$ permanently binds iron atoms, rendering them inactive in the redox cycle, as this compound is not reducible under the applied reaction conditions [36]. In contrast, Takenaka et al. [37] demonstrated that Mo cations in $Mo_xFe_{3-x}O_4$ actively participate in the redox cycle. While this contributes to the hydrogen storage capacity, the associated redox activity may increase the mobility of the phase within the material [38], potentially making it a less effective inhibitor of surface diffusion and consequently sintering. Since hydrogen production of FeOx-Mo does not cease by the end of the tenth cycle, a decline in performance with continued redox cycling can be expected.

In the first cycle, FeOx-98 showed slightly lower initial H_2 concentrations (10 vol.—%) but similar oxidation behavior to Al-modified FeOx. After ten cycles, the H_2 peak decreased by 17 %, and the oxidation duration extended by 6 min. Following the initial peak, the H_2 concentration decreases, however after about 8 min it increases slightly and stabilizes for approximately 5 min before the final decline. This brief increase may be attributed to pronounced crack formation in the pellet during the later stages of oxidation, as shown in Fig. 7. The significantly higher oxidation rate in the tenth cycle of FeOx-98 pellets compared to high-purity FeOx pellets indicates a degree of stabilization by the small amounts of Al and Cr present [15,20]. In addition, morphological effects are likely to contribute to this behavior [39].

To facilitate comparison of the H_2 storage performance among the modified oxides, Fig. 5 presents the accumulative amount of H_2 produced per oxidation step. For better comparability, the amount of H_2 produced is normalized to the mass of iron. The maximum theoretical H_2 production, corresponding to complete oxidation of Fe to Fe_3O_4, is 23.9 mmol g_{Fe}^{-1}. In addition, the corresponding iron conversion during oxidation is indicated, where a conversion of 0 % represents fully reduced metallic iron and 100 % denotes complete oxidation to Fe_3O_4.

The high-purity iron oxide pellets (FeOx) exhibited rapid deactivation, with H_2 production decreasing from 21.2 mmol g_{Fe}^{-1} (89 % Fe conversion) in the first cycle to 5.0 mmol g_{Fe}^{-1} in the tenth, corresponding to a performance loss of over 75 %. This decline is attributed to sintering and pore closure [18,21]. The observed decline in hydrogen production is very close to the behavior of Fe_2O_3 powder. In our former study [21], we observed the same initial hydrogen production with Fe_2O_3 powder as in this work and a decrease to 9 mmol g_{Fe}^{-1}, compared to a decline to 10 mmol g_{Fe}^{-1} within five cycles. This indicates that the pelletization alone does not significantly prevent material degradation.

In contrast, the addition of all Al and Mo additives stabilizes hydrogen production over multiple cycles. FeOx-Mo showed the highest initial activity (23.9 mmol g_{Fe}^{-1}) and retained 92 % of its performance after ten cycles. Full conversion of Fe to Fe_3O_4 was observed in the first few cycles, followed by slight decline. The high level of H_2 production might be attributed to the redox activity of molybdenum oxides [15,17,21,37]. The amount of hydrogen produced by FeOx-Mo pellets is 5 % to 13 % higher than that observed for powder samples [21]. This difference is likely attributable to variations in reaction parameters, such as volumetric flow rate and reaction time. In a previous powder-based study [21], the long-term stability of Mo-modified iron oxide was examined, revealing a 28 % decline in hydrogen production over 50 cycles. Since oxidation of FeOx-Mo pellets was not completed by the end of the tenth cycle, a similar decline, as observed for the powder samples, can be expected for the pelletized material with continued cycling.

FeOx-Al exhibited slightly lower initial H_2 production (22.6 mmol g_{Fe}^{-1}), which decreased by 6 % over ten cycles. The incomplete conversion of iron might be attributed to the formation of mixed iron-aluminum oxides, which limit the fraction of redox-active iron [36]. The hydrogen production during oxidation of Al-modified iron oxide powder is very similar to the H_2 production observed in this work. In the first cycle, 21.6 mmol g_{Fe}^{-1} was produced, and a decline of 5 % was observed over ten cycles [21]. These results indicate that the stabilizing effects of Mo and Al doping in iron oxide observed for powder systems can be transferred to pelletized materials for fixed-bed applications.

Increasing the induration temperature to 1300 °C (FeOx-Al(HT)) improved its resistance toward sintering. Despite the lower initial hydrogen production (20.5 mmol g_{Fe}^{-1}), this sample maintained its performance over cycling and even showed a slight increase of 4 % in H_2 production. This increase in hydrogen production with increasing cycle number is in contrast to the other iron oxide pellets show a decline of different magnitudes. Therefore, FeOx-Al(HT) exhibits the same level of hydrogen production as FeOx-Al and FeOx-Mo in the tenth cycle. Especially the different behavior of the Al-modified iron oxides indurated at different temperature are indicating, that the stabilizing effect is also affected by thermal treatment prior to redox cycling.

Overall, the lower-purity iron oxide (FeOx-98), containing trace impurities of Al (0.06 %) and Cr (0.05 %), exhibited the highest level of H_2 production over ten cycles. During the first oxidation 23.4 mmol g_{Fe}^{-1} of H_2 were produced, close to complete iron conversion with only 0.7 % performance loss over ten cycles. Its impurities, Al and Cr are known to enhance sintering resistance in the steam-iron process [15,20,21].

The stabilizing effect of Al is due to $FeAl_2O_4$ formation [36], while Cr was shown to be stabilized in $Cr_xFe_{3-x}O_4$ [40]. If located on the surface, these ferrites would inhibit contact between the iron (oxide) particles and mitigate neck growth [18,40]. However, Lorente et al. [20] found an additive loading of 5 mol% for Al and Cr to be optimal for maintaining a high hydrogen storage capacity. This optimal additive loading is ≈ 50 times higher than the trace impurities included in this iron oxide. Consequently, the low-concentration Al and Cr may contribute to the observed stability but are not the sole stabilizing factor. The superior stability of FeOx-98 compared to synthetically modified oxides suggests that additional factors, such as primary particle size and morphology, play a decisive role in controlling sintering behavior [39]. Fig. 6 shows SEM images of the two different iron oxide materials. Fe_2O_3(98 %), used for FeOx98, displays

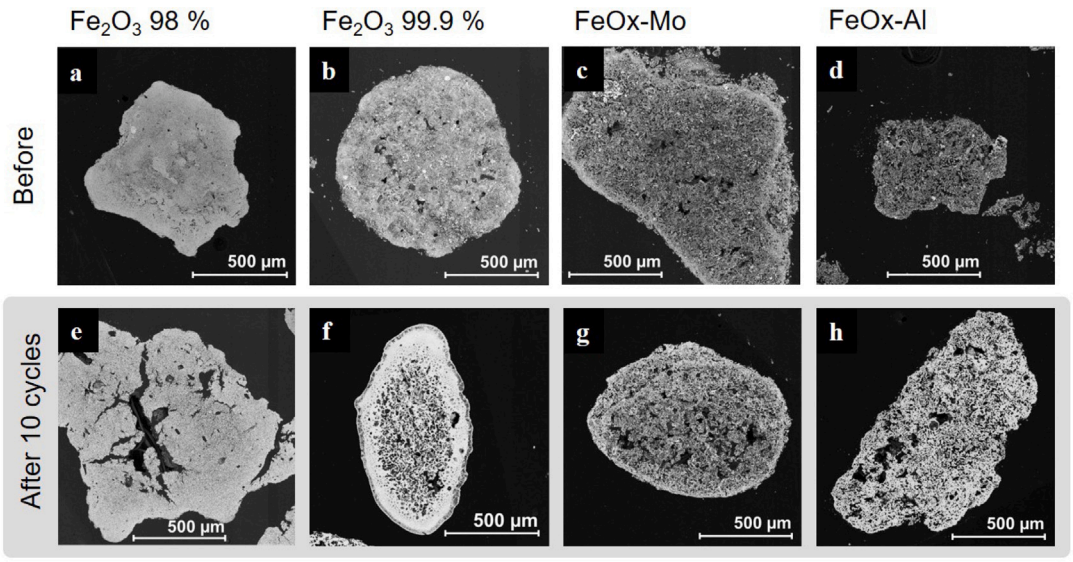

Fig. 7. Cross-sectional SEM images of iron oxide pellets before (a-d) and after ten (e-h) redox cycles: (a,e) FeOx, (b,f) FeOx-98, (c,g) FeOx-Mo and (d,h) FeOx-Al indurated at 700 °C.

Table 1
Specific surface area of iron oxide pellets before and after ten cycles.

Sample	Specific surface area/ $\frac{m^2}{g}$		Change/%
	Before	After 10 cycles	
FeOx	2.64	0.61	−77
FeOx-Mo	2.35	1.31	−44
FeOx-Al	6.97	3.21	−54
FeOx-Al(HT)	0.69	1.23	+79
FeOx98	4.82	3.30	−31

a narrow size distribution and predominantly spherical particles. In contrast, Fe_2O_3(99.9 %), used for all other pellets, exhibits a broad size distribution with irregular, flake-like particle shapes. Particle size and morphology are decisive for the sintering rate. Irregular, flake-shaped particles provide a larger contact area and promote faster densification, whereas spherical particles reduce contact points and decelerate sintering [39,41].

3.3. Structural evolution

The trends shown by the accumulated hydrogen production per cycle are also reflected in the morphological changes.

The specific surface area of the samples before and after ten cycles is shown in Table 1. While FeOx shows a 77 % decline in specific surface area, FeOx-Al declines by 54 %, FeOx-Mo by 44 % and FeOx-98 only by 31 %. After ten cycles, FeOx-Al(HT) even shows an increase in specific surface area by 79 %. The surface area decline exhibits the same trend as reported for the powder [21].

Cross-sectional SEM images reveal pronounced changes in pellet morphology after ten redox cycles (Fig. 7). Pure iron oxide developed a dense outer layer approximately 100 µm thick, accompanied by significant coarsening of the internal pore structure. This observation clearly indicates progressive sintering during repeated reduction and oxidation. The formation of a compact outer shell may impose diffusion limitations, thereby contributing to the observed decline in Fe conversion with increasing cycle number.

In contrast, the modified iron oxides exhibit less severe sintering. Mo-modified iron oxides show moderate structural coarsening after ten cycles and slight surface densification, however, a continuous dense shell is not formed, unlike in pure FeOx. Prior to cycling, Al-modified iron oxide pellets appear less compact than the other materials and exhibit a highly porous, loosely connected microstructure. The weak interparticle connectivity leads to the observed reduced mechanical stability. After ten cycles, the structure evolves into a coarser framework characterized by macropores in the range of 5 µm to 50 µm, while retaining mesoporous oxide walls. Compared to the Mo-modified material, visible sintering is slightly more pronounced, consistent with the slightly greater decline in specific surface area.

FeOx-98 pellets, in contrast, appear more densely packed prior to cycling. After redox cycling, only limited sintering is observed, however, crack and cavity formation within the pellets becomes evident. The development of such cracks may facilitate gas transport to and from the pellet core, potentially contributing to the stable hydrogen storage performance of FeOx-98.

Furthermore, the structural evolution of Al-stabilized iron oxide during redox cycling is influenced by the induration temperature applied during pellet preparation (Fig. 8). FeOx-Al(HT), indurated at 1300 °C, initially exhibits a coarse macroporous structure with dense walls. The elevated induration temperature promotes particle agglomeration, resulting in a denser microstructure compared to pellets indurated at 700 °C. After cycling, the macroporous framework is largely preserved, while wall porosity increases. This increase is more clearly visible in the surface SEM images (Fig. 8 e-f). Together with the measured increase in specific surface area, these observations indicate that redox cycling of FeOx-Al(HT) promotes pore formation rather than sintering. Pore generation may occur via oxygen removal during reduction [42,43] or through outward diffusion of $Fe^{2+/3+}$ ions during oxidation [44,45]. While these mechanisms are expected to occur in all investigated materials, sintering remains the dominant process governing morphological evolution in the other pellets. The contrasting behavior of FeOx-Al(HT), characterized by increased porosity, can be attributed to two main factors. First, the initial microstructure is already more sintered, therefore consisting of larger primary particles. Since sintering rates generally increase with decreasing particle size [46], the larger primary particles in FeOx-Al(HT) relative to pellets indurated at 700 °C likely result in a reduced sintering rate during cycling. Second, the higher induration temperature facilitates the formation of α-Al_2O_3. The transformation from metastable γ-Al_2O_3 to α-Al_2O_3 may play a critical role in mitigating sintering processes [36,47]. The associated increase in porosity and specific surface area likely contributes to the progressive improvement in Fe conversion observed with increasing cycle number.

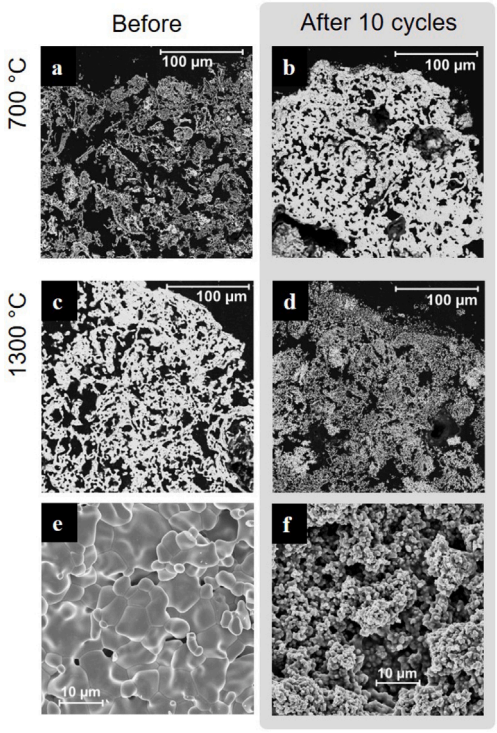

Fig. 8. Cross-sectional SEM images of Al-stabilized iron oxide pellets before and after ten redox cycles with an induration temperature of (a-b) 700 °C and (c-f) 1300 °C. (e-f) show surface SEM images of FeOx-Al(HT) indurated at 1300 °C.

4. Conclusion

This study demonstrates that iron oxide-based pellets can effectively serve as cyclic hydrogen storage materials in the steam-iron process. Observed trends confirm that stabilization mechanisms known in powder systems also apply to mechanically stable pellets. Pure Fe_2O_3 rapidly deactivated due to sintering, however the incorporation of small amounts of stabilizing additives or impurities markedly enhanced performance and durability. Impure iron oxide containing traces Al and Cr, exhibited the highest stability and nearly complete iron conversion over ten cycles. This emphasizes that even dopant concentrations below 0.1 % can significantly improve long-term redox stability. Furthermore, the primary particle size and shape of the iron oxide is decisive for cyclability, and morphological changes such as crack formation can facilitate gas transport into the center of the pellet. Mo-modified iron oxide exhibited full conversion up to the fourth cycle, thereafter its hydrogen production declined slowly. Sintering inhibition was slightly improved over Al-modified iron oxide indurated at 700 °C. The Al-modified iron oxide indurated at 1300 °C was the most effective in suppressing sintering. Pore formation during redox cycling dominated over sintering, leading to increased porosity and enhanced H_2 production with successive cycles. Although its initial H_2 yield was slightly lower, the upward trend indicates strong potential for long-term stability. While this work demonstrates trends over ten cycles, the relevance for practical applications requires assessment over more cycles. Literature on Mo-doped powders indicates that after 50 cycles the hydrogen storage capacity drops by 28 %, therefore similar behavior can be expected for the pellets investigated in this work. Consequently, a long-term study of the FeOx-Al(HT) pellets is necessary to verify whether a stable plateau can be achieved or if a performance decline is delayed.

CRediT authorship contribution statement

Anna Knapp: Writing – original draft, Investigation, Formal analysis, Conceptualization. **Robin Flügel:** Investigation, Formal analysis. **Felix Straub:** Writing – review & editing, Investigation. **Olaf Deutschmann:** Writing – review & editing, Supervision, Funding acquisition, Conceptualization.

Declaration of Generative AI and AI-assisted technologies in the writing process

During the preparation of this work, the authors used ChatGPT and DeepL Write in order to improve readability. After using this tool/service, the authors reviewed and edited the content as needed and take full responsibility for the content of the publication.

Declaration of competing interest

The authors declare that they have no known competing financial interests or personal relationships that could have appeared to influence the work reported in this paper.

Acknowledgments

This work was conducted within the Clean Circles cluster project and supported by the KIT Strategy Fund. Financial support by the DFG (German Research Foundation), project numbers 441926934 and 558715615, is acknowledged. The authors gratefully acknowledge Jonas Kaltenbach (LEM, KIT) for performing the SEM measurements and Sandeep Kurukunda (ITCP, KIT) for conducting the BET measurements. The authors also thank the group of Manfred Wilhelm (ITCP, KIT) for providing access to the universal testing machine, and especially Max Schußmann for his support in operating the equipment.

References

[1] J.M. Bergthorson, Recyclable metal fuels for clean and compact zero-carbon power, Prog. Energy Combust. Sci. 68 (2018) 169–196.
[2] M. Baumann, L. Barelli, S. Passerini, The potential role of reactive metals for a clean energy transition, Adv. Energy Mater. 10 (27) (2020) 2001002.
[3] P. Debiagi, R. Rocha, A. Scholtissek, J. Janicka, C. Hasse, Iron as a sustainable chemical carrier of renewable energy: Analysis of opportunities and challenges for retrofitting coal-fired power plants, Renew. Sustain. Energy Rev. 165 (2022) 112579.
[4] L. Dirven, N.G. Deen, M. Golombok, Dense energy carrier assessment of four combustible metal powders, Sustain. Energy Technol. Assess. 30 (2018) 52–58.
[5] C. Kuhn, A. Düll, P. Rohlfs, S. Tischer, M. Börnhorst, O. Deutschmann, Iron as recyclable energy carrier: Feasibility study and kinetic analysis of iron oxide reduction, Appl. Energy Combust. Sci. 12 (2022) 100096.
[6] L. Braun, J. Spielmann, D.E. Doronkin, C. Kuhn, A. Maliugin, D.I. Sharapa, I. Huck, J. Bao, S. Tischer, F. Studt, O. Deutschmann, U.I. Kramm, J.-D. Grunwaldt, Following the structural changes of iron oxides during reduction under transient conditions, ChemSusChem (2024) e202401045.
[7] J. Janicka, P. Debiagi, A. Scholtissek, A. Dreizler, B. Epple, R. Pawellek, A. Maltsev, C. Hasse, The potential of retrofitting existing coal power plants: A case study for operation with green iron, Appl. Energy 339 (2023) 120950.
[8] C. Kuhn, M. Kirn, S. Tischer, O. Deutschmann, Micron-sized iron particles as energy carrier: Cycling experiments in a fixed-bed reactor, Proc. Combust. Inst. 40 (1–4) (2024) 105207.
[9] J.M. Bergthorson, Y. Yavor, J. Palecka, W. Georges, M. Soo, J. Vickery, S. Goroshin, D.L. Frost, A.J. Higgins, Metal-water combustion for clean propulsion and power generation, Appl. Energy 186 (2017) 13–27.
[10] P. Lott, O. Deutschmann, Heterogeneous chemical reactions—A cornerstone in emission reduction of local pollutants and greenhouse gases, Proc. Combust. Inst. 39 (3) (2023) 3183–3215.
[11] P. Julien, J.M. Bergthorson, Enabling the metal fuel economy: green recycling of metal fuels, Sustain. Energy Fuels 1 (3) (2017) 615–625.
[12] A. Messerschmitt, Process of producing hydrogen, 1910, US Patent 971206A, Assigned to Corp Internationale Wasserstoff AG.
[13] S. Hurst, Production of hydrogen by the steam-iron method, Oil Soap 16 (2) (1939) 29–35.

[14] L. Brinkman, B. Bulfin, A. Steinfeld, Thermochemical hydrogen storage via the reversible reduction and oxidation of metal oxides, Energy Fuels 35 (22) (2021) 18756–18767.
[15] K. Otsuka, T. Kaburagi, C. Yamada, S. Takenaka, Chemical storage of hydrogen by modified iron oxides, J. Power Sources 122 (2) (2003) 111–121.
[16] K. Müller, Technologies for the storage of hydrogen Part 1: Hydrogen storage in the narrower sense, ChemBioEng Rev. 6 (3) (2019) 72–80.
[17] M. Thaler, V. Hacker, Storage and separation of hydrogen with the metal steam process, Int. J. Hydrog. Energy 37 (3) (2012) 2800–2806.
[18] V. Galvita, T. Hempel, H. Lorenz, L.K. Rihko-Struckmann, K. Sundmacher, Deactivation of modified iron oxide materials in the cyclic water gas shift process for CO-free hydrogen production, Ind. Eng. Chem. Res. 47 (2) (2008) 303–310.
[19] K. Otsuka, C. Yamada, T. Kaburagi, S. Takenaka, Hydrogen storage and production by redox of iron oxide for polymer electrolyte fuel cell vehicles, Int. J. Hydrog. Energy 28 (3) (2003) 335–342.
[20] E. Lorente, J. Peña, J. Herguido, Separation and storage of hydrogen by steam-iron process: Effect of added metals upon hydrogen release and solid stability, J. Power Sources 192 (1) (2009) 224–229.
[21] A. Knapp, C. Kuhn, O. Deutschmann, Hydrogen storage in modified iron oxides: The effect of additives on the cyclic stability, Fuel 404 (2026) 136200.
[22] L. Huber, M. Heindl, M. Schlosser, A. Pfitzner, B. Dawoud, On the cycle stability and macroscopic structure of iron oxide pellets for thermochemical hydrogen storage: Influence of water content during the pelletizing process, Appl. Sci. 13 (11) (2023) 6408.
[23] S.K. Kawatra, V. Claremboux, Iron ore pelletization: Part i. Fundamentals, Miner. Process. Extr. Met. Rev. 43 (4) (2022) 529–544.
[24] J. Pal, S. Ghoari, A. Ammasi, S. Hota, V. Koranne, T. Venugopalan, Improving reducibility of iron ore pellets by optimization of physical parameters, J. Min. Met. Sect. B: Met. 53 (1) (2017) 37–46.
[25] H. Gossler, J. Riedel, E. Daymo, R. Chacko, S. Angeli, O. Deutschmann, A new approach to research data management with a focus on traceability: Adacta, Chem. Ing. Tech. 94 (11) (2022) 1798–1807.
[26] D. Spreitzer, J. Schenk, Reduction of iron oxides with hydrogen—A review, Steel Res. Int. 90 (10) (2019) 1900108.
[27] Q. Fradet, M. Kurnatowska, U. Riedel, Thermochemical reduction of iron oxide powders with hydrogen: Review of selected thermal analysis studies, Thermochim. Acta 726 (2023) 179552.
[28] L. Choisez, K. Hemke, Ö. Özgün, C. Pistidda, H. Jeppesen, D. Raabe, Y. Ma, Hydrogen-based direct reduction of combusted iron powder: Deep pre-oxidation, reduction kinetics and microstructural analysis, Acta Mater. 268 (2024) 119752.
[29] P. Cavaliere, L. Dijon, A. Laska, D. Koszelow, Hydrogen direct reduction and reoxidation behaviour of high-grade pellets, Int. J. Hydrog. Energy 49 (2024) 1235–1254.
[30] J.A. Halt, S.K. Kawatra, Does the zeta potential of an iron ore concentrate affect the strength and dustiness of unfired and fired pellets? Miner. Process. Extr. Met. Rev. 38 (2) (2017) 132–141.
[31] M. Simnad, A. Spilners, Kinetics and mechanism of the oxidation of molybdenum, J. Met. 7 (9) (1955) 1011–1016.
[32] N. Nurdini, M.M. Ilmi, E. Maryanti, P. Setiawan, G.T.M. Kadja, Ismunandar, Thermally-induced color transformation of hematite: insight into the prehistoric natural pigment preparation, Heliyon 8 (8) (2022) e10377.
[33] P. Franklin, B.L. Davies, The effects of steam oxidation on porosity in sintered iron, Powder Metall. 20 (1) (1977) 11–16.
[34] T.E. Mitchell, D.A. Voss, E.P. Butler, The observation of stress effects during the high temperature oxidation of iron, J. Mater. Sci. 17 (6) (1982) 1825–1833.
[35] R. Stehle, M. Bobek, R. Hooper, D. Hahn, Oxidation reaction kinetics for the steam-iron process in support of hydrogen production, Int. J. Hydrog. Energy 36 (23) (2011) 15125–15135.
[36] P.R. Kidambi, J.P.E. Cleeton, S.A. Scott, J.S. Dennis, C.D. Bohn, Interaction of iron oxide with alumina in a composite oxygen carrier during the production of hydrogen by chemical looping, Energy Fuels 26 (1) (2012) 603–617.
[37] S. Takenaka, T. Kaburagi, C. Yamada, K. Nomura, K. Otsuka, Storage and supply of hydrogen by means of the redox of the iron oxides modified with Mo and Rh species, J. Catalysis 228 (1) (2004) 66–74.
[38] Y. Dong, Redox enhanced slow ion kinetics in oxide ceramics, J. Am. Ceram. Soc. 107 (3) (2024) 1905–1916.
[39] M.R. Mazlan, N.H. Jamadon, A. Rajabi, A.B. Sulong, I.F. Mohamed, F. Yusof, N.A. Jamal, Necking mechanism under various sintering process parameters – A review, J. Mater. Res. Technol. 23 (2023) 2189–2201.
[40] S. Takenaka, N. Hanaizumi, V.T.D. Son, K. Otsuka, Production of pure hydrogen from methane mediated by the redox of Ni- and Cr-added iron oxides, J. Catalysis 228 (2) (2004) 405–416.
[41] K. Miyake, Y. Hirata, T. Shimonosono, S. Sameshima, The effect of particle shape on sintering behavior and compressive strength of porous alumina, Materials 11 (7) (2018) 1137.
[42] E.T. Turkdogan, R.G. Olsson, J.V. Vinters, Gaseous reduction of iron oxides: Part II. Pore characteristics of iron reduced from hematite in hydrogen, Met. Trans. 2 (11) (1971) 3189–3196.
[43] X. Zhou, Y. Bai, A.A. El-Zoka, S.-H. Kim, Y. Ma, C.H. Liebscher, B. Gault, J.R. Mianroodi, G. Dehm, D. Raabe, Effect of pore formation on redox-driven phase transformation, Phys. Rev. Lett. 130 (16) (2023) 168001.
[44] F. Li, Z. Sun, S. Luo, L.-S. Fan, Ionic diffusion in the oxidation of iron—effect of support and its implications to chemical looping applications, Energy Environ. Sci. 4 (3) (2011) 876.
[45] R. Chen, W. Yeun, Review of the high-temperature oxidation of iron and carbon steels in air or oxygen, Oxid. Met. 59 (5) (2003) 433–468.
[46] N. Kothari, The effect of particle size on sintering kinetics in alumina powder, J. Nucl. Mater. 17 (1) (1965) 43–53.
[47] I. Levin, D. Brandon, Metastable alumina polymorphs: Crystal structures and transition sequences, J. Am. Ceram. Soc. 81 (8) (1998) 1995–2012.